

Structural, magnetic and electrical properties of sputter deposited Mn-Fe-Ga thin films

Alessia Niesen¹, Christian Sterwerf¹, Manuel Glas¹, Jan-Michael Schmalhorst¹ and Günter Reiss¹

¹Center for Spinelectronic Materials and Devices, Physics Department, Bielefeld University, Germany

Abstract—We investigated structural, magnetic and electrical properties of sputter deposited Mn-Fe-Ga compounds. The crystallinity of the Mn-Fe-Ga thin films was confirmed using x-ray diffraction. X-ray reflection and atomic force microscopy measurements were utilized to investigate the surface properties, roughness, thickness and density of the deposited Mn-Fe-Ga. Depending on the stoichiometry, as well as the used substrates (SrTiO₃ (001) and MgO (001)) or buffer layer (TiN) the Mn-Fe-Ga crystallizes in the cubic or the tetragonally distorted phase. Anomalous Hall effect and alternating gradient magnetometry measurements confirmed strong perpendicular magnetocrystalline anisotropy. Low saturation magnetization and hard magnetic behavior was reached by tuning the composition. Temperature dependent anomalous Hall effect measurements in a closed cycle He-cryostat showed a slight increase in coercivity with decreasing temperature (300 K to 2 K). TiN buffered Mn_{2.7}Fe_{0.3}Ga revealed sharper switching of the magnetization compared to the unbuffered layers.

Index Terms—Heusler compounds, perpendicular magnetocrystalline anisotropy, magnetic properties, material science, spintronics

I. INTRODUCTION

Ferromagnetic, fully spin polarized materials (half-metals) found a lot of interest in the recent years due to their possible application in spintronic devices as nonvolatile memories [1] and field programmable logic devices. [2], [3] To maintain the thermal stability at shrinking device sizes, an out-of-plane (oop) oriented magnetization of the material is advantageous. Therefore investigation of perpendicularly magnetized Heusler compounds has found attraction. High spin polarization and out-of-plane magnetization direction was predicted for the Mn_{3-x}Ga (0.15 ≤ x ≤ 2) compound. [4]–[6] The transition from the cubic D0₃ into the tetragonal D0₂₂ phase takes place at temperatures above 500°C. [7] Hence a variation of the deposition temperature is an important criterium in terms of the crystallographic properties. The tetragonally distortion could also be obtained by shifting the Fermi energy at the Van Hove singularity in one of the spin-channels, which is reached by tuning the material with an additional element. [8] Mn-Fe-Ga is one possible material, which is calculated to be 95 % spin polarized at the Fermi level for the cubic phase (Mn₂Fe₁Ga). [9] The predicted low total magnetization $M = 1.03 \mu_B$ [9] and high Curie temperature $T_C = 550$ K (lowest measured value for Mn_{1.4}Fe_{1.6}Ga) makes this material an interesting candidate to serve as an electrode in magnetic tunnel junctions (MTJ's). [10] Additionally, depending on the composition Mn-Fe-Ga shows magnetocaloric effects. [8] In this work, we focused on the preparation and investigation

of the crystallographic, structural, electrical and magnetic properties of the ternary Mn-Fe-Ga compound. The influence of different substrates and deposition temperatures on the material properties was investigated. With regard to the preparation of magnetic tunnel junctions and the aim to increase their applicability a TiN seed-layer was used. Sputter deposited TiN is a material with low electrical resistivity (16 μΩ cm) and a surface roughness below 1 nm. [11], [12] Thus it provides a good electrical connection to the MTJ. High thermal stability (melting point 2950 °C [13]) is another advantage, which prevents chemical reactions of TiN with the on top deposited material. The lattice constant of TiN (fcc structure) is 4.24 Å and therefore suitable for various Heusler compounds. It was already shown, that TiN is a suitable seed-layer for Mn_{3-x}Ga and Co₂FeAl. [14]

II. EXPERIMENTAL

Mn-Fe-Ga thin films (40 nm thickness) were prepared in a UHV sputtering system with a base pressure below 5×10^{-10} mbar. DC magnetron co-sputtering from a pure Mn, Fe and a Mn₄₅Ga₅₅ composite target was used to prepare the samples. The Ar pressure was set to 1.7×10^{-3} mbar. Different stoichiometries were achieved by varying the power values between 10 W and 200 W during sputtering. Deposition temperatures from 280 °C to 595 °C were chosen in order to achieve high crystallinity and the tetragonally distorted phase. MgO (100) and SrTiO₃ (STO) (100) single crystalline substrates were utilized. Additionally TiN buffered Mn-Fe-Ga thin films on MgO and STO substrates were prepared. The TiN layers (30 nm) were deposited using reactive sputtering in an Argon - Nitrogen atmosphere which results in stoichiometric Ti₁N₁ thin films. During the sputtering process a N flow of 2 sccm and an Ar flow of 20 sccm was used, leading to a deposition pressure of 1.6×10^{-3} mbar. On top of the Heusler compound a 2 nm thick MgO layer was deposited to coat surface contaminations.

III. CHARACTERIZATION OF THE MN-FE-GA COMPOUND

A. Crystal structure

Crystallographic properties of the Mn-Fe-Ga thin films were determined via x-ray diffraction (XRD) and x-ray reflection (XRR) measurements using a XRD Philips X'Pert Pro diffractometer (Cu anode). The lowest roughness values (≤ 1 nm) combined with the highest crystallinity were measured on samples deposited at temperatures of 407 °C and 450 °C. The transition from the cubic D0₃ into the tetragonally distorted

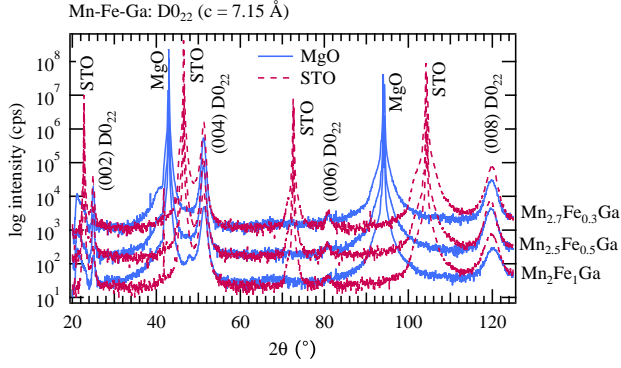


Fig. 1. XRD patterns of the $\text{Mn}_{3-x}\text{Fe}_x\text{Ga}$ compound deposited at 450°C on MgO (blue) and SrTiO_3 (red) substrates.

D0₂₂ phase takes place at deposition temperatures above 322°C . All samples with the $\text{Mn}_{3-x}\text{Fe}_x\text{Ga}$ ($0.3 \leq x \leq 1$) stoichiometry crystallize in the D0₂₂ tetragonally distorted phase (Fig. 1) which is in good agreement with the previously reported data. [10] The determined out-of-plane lattice constant c is 7.15 \AA for Mn-Fe-Ga deposited on both substrate types. Increasing the Fe and decreasing the Mn amount leads to a formation of the cubic phase (D0₃) ($c = 5.95 \text{ \AA}$) on MgO substrates (not shown). On STO each composition results in a formation of the tetragonally distorted phase, due to the low lattice mismatch of 0.5% with the in-plane lattice constant ($a = 3.89 \text{ \AA}$) of Mn-Fe-Ga. Deposition on a TiN buffer layer leads to a mixture of the cubic D0₃ and the tetragonally distorted D0₂₂ phase depending on the Mn-Fe-Ga composition (not shown). $\text{Mn}_{2.7}\text{Fe}_{0.3}\text{Ga}$ crystallizes only in the tetragonally distorted phase at deposition temperatures above 288°C on a TiN seed-layer. With increasing Fe amount (decreasing Mn amount) the ratio of the cubic phase increases. For films with an Fe amount of $1 \leq x$ only the cubic phase is formed. The density of the samples was determined via XRR measurements and also revealed a dependence on the crystallographic phase. The density of the tetragonally distorted Mn-Fe-Ga is $7.1 \pm 0.5 \text{ g/cm}^3$ and $6 \pm 0.5 \text{ g/cm}^3$ for the cubic phase.

B. Surface properties

Atomic force microscopy (AFM) was carried out to investigate the surface topology of the samples. The grain structure of the thin films shows a strong dependence on the stoichiometry, on the deposition temperature and the used substrate. Fig. 2 shows a comparison of a tetragonally distorted $\text{Mn}_{2.7}\text{Fe}_{0.3}\text{Ga}$ and a cubic $\text{Fe}_{2.6}\text{Mn}_{1.2}\text{Ga}$ layer deposited on MgO at 450°C . The $\text{Mn}_{2.7}\text{Fe}_{0.3}\text{Ga}$ forms $200 \text{ nm} - 400 \text{ nm}$ grains with steep grain boundaries. The measured roughness value is $3.4 \pm 0.05 \text{ nm}$. The cubic $\text{Fe}_{2.6}\text{Mn}_{1.2}\text{Ga}$ compound forms small grains and a smooth surface (roughness = $0.8 \pm 0.05 \text{ nm}$). Mn-Fe-Ga with decreased Mn ratio shows island growth (Fig. 3). The grains seem to be disconnected from each other, which leads to a roughness value of $17 \pm 0.5 \text{ nm}$. The equivalent film (temperature and stoichiometry) on STO revealed no island growth and low roughness of $0.43 \pm 0.05 \text{ nm}$

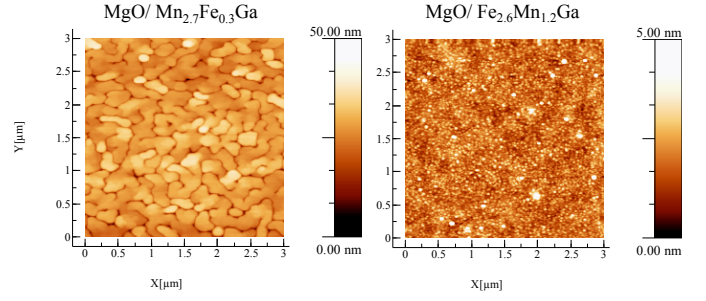


Fig. 2. AFM images of $\text{Mn}_{2.7}\text{Fe}_{0.3}\text{Ga}$ (tetragonally distorted phase) and $\text{Fe}_{2.6}\text{Mn}_{1.2}\text{Ga}$ (cubic phase) thin films deposited on MgO (100) substrates at 450°C .

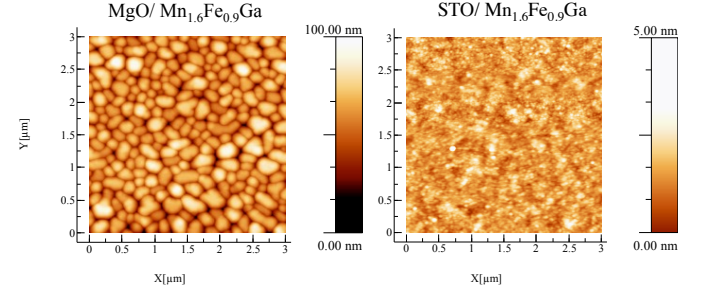


Fig. 3. AFM images of $\text{Mn}_{1.6}\text{Fe}_{0.9}\text{Ga}$ (tetragonally distorted) deposited on MgO (100) and STO (100) substrates at 550°C .

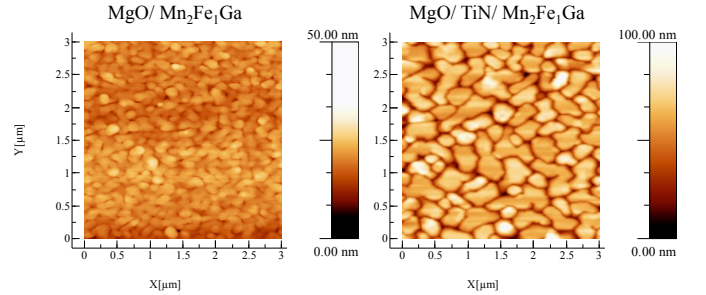


Fig. 4. AFM images of $\text{Mn}_2\text{Fe}_1\text{Ga}$ deposited on MgO (100) at 550°C without (tetragonal) and with (cubic) a TiN buffer layer.

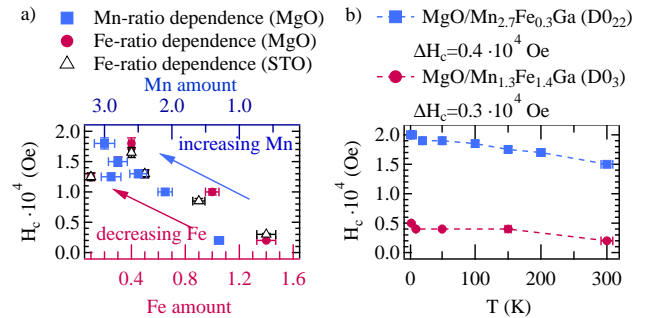


Fig. 5. a) Coercivity dependence on the Mn (blue squares) or Fe (red circles/black triangles) ratio for Mn-Fe-Ga deposited on MgO and STO substrate. b) Temperature dependence of the H_c for tetragonally distorted (blue squares) and cubic (red circles) Mn-Fe-Ga samples deposited on MgO.

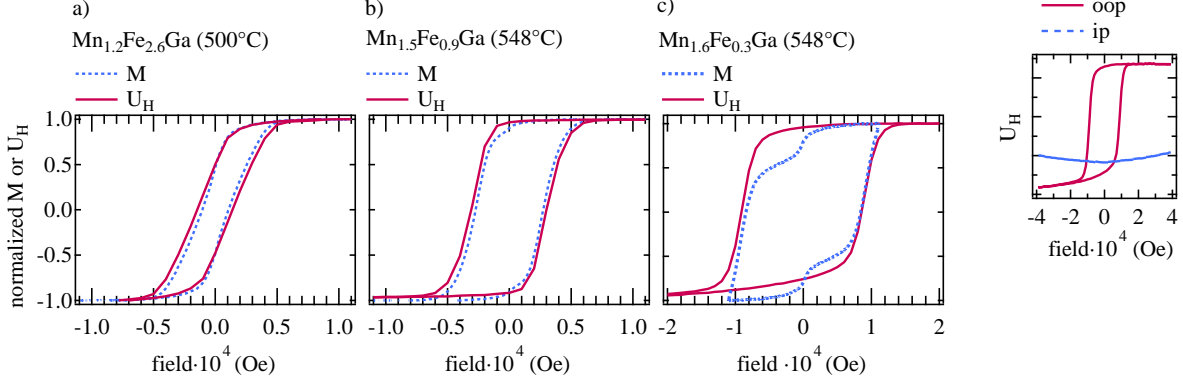


Fig. 6. Out-of-plane measured AHE (red) and AGM (blue) hysteresis curves for a) $\text{Mn}_{1.2}\text{Fe}_{2.6}\text{Ga}$, b) $\text{Mn}_{1.5}\text{Fe}_{0.9}\text{Ga}$ and c) $\text{Mn}_{1.6}\text{Fe}_{0.3}\text{Ga}$ thin films deposited on STO at 500 °C and 548 °C. The measured magnetization M and Hall voltage values U_H are normalized for a better comparison. The additional graph shows an ip and oop AHE hysteresis curve for $\text{Mn}_{1.6}\text{Fe}_{0.3}\text{Ga}$ deposited on STO.

(Fig. 3), which can be attributed to the low lattice mismatch with the in-plane lattice constant of the tetragonally distorted Mn-Fe-Ga. Island growth occurs if the surface energy of the substrate is lower than the sum of the surface energies of the film and the interface. In this case growth on atomic layers is energetically favoured and the deposited material forms islands. Films deposited on a TiN seed-layer also showed island growth and high roughness (14.25 ± 0.05 nm) (Fig. 4). As previously mentioned, TiN buffered $\text{Mn}_2\text{Fe}_1\text{Ga}$ crystallizes in the cubic D0_3 phase. The lattice mismatch with TiN, assuming 45 degree rotated growth, is 0.7%. Nevertheless, the sample revealed island growth and steep grain boundaries. Therefore the surface energy of TiN needs to be lower than the surface energy of Mn-Fe-Ga together with the interface energy. Reducing the sputter rate of Mn-Fe-Ga could lead to a decrease of the surface energy as well as the interface energy and therefore prevent island growth.

C. Magnetic and electrical properties

The magnetic properties were investigated via AGM (alternating gradient magnetometry) and AHE (anomalous Hall effect) measurements. High coercivity fields ($H_c \leq 2 \cdot 10^4$ Oe) in the oop direction can be reached by tuning the composition. The coercivity increases with decreasing Fe and increasing Mn amount (Fig. 5 a). Temperature dependent AHE measurements in a closed cycle He-cryostat showed a slight increase of the coercivity $\Delta H_c = 0.4 \cdot 10^4$ Oe for tetragonally distorted $\text{Mn}_{2.7}\text{Fe}_{0.3}\text{Ga}$ and $\Delta H_c = 0.3 \cdot 10^4$ Oe for the cubic $\text{Mn}_{1.3}\text{Fe}_{1.4}\text{Ga}$ with decreasing temperature (300 K to 2 K) (Fig. 5 b). Each sample revealed a hard magnetic axis in the in-plane direction. An example of an in- and out-of-plane AHE hysteresis curve for $\text{Mn}_{1.6}\text{Fe}_{0.3}\text{Ga}$ is shown in Fig. 6 (additional graph). Since the samples could not be saturated in the in-plane direction even at an applied field of $4 \cdot 10^4$ Oe a strong perpendicular magnetocrystalline anisotropy (PMA) is experimentally verified. Fig. 6 shows a comparison of normalized magnetization M and AHE curves (U_H). In case of the $\text{Mn}_{1.2}\text{Fe}_{2.6}\text{Ga}$ and $\text{Mn}_{1.5}\text{Fe}_{0.9}\text{Ga}$ deposited on STO substrates the hysteresis curves are in good agreement. The

coercivity is $0.1 \cdot 10^4$ Oe for $\text{Mn}_{1.2}\text{Fe}_{2.6}\text{Ga}$ and $0.3 \cdot 10^4$ Oe for $\text{Mn}_{1.5}\text{Fe}_{0.9}\text{Ga}$. The squareness ratio $S_R = M_r/M_s$ or $S_R = \rho_{yxr}/\rho_{yxs}$ (the r or s index denotes the remanence or the saturation value of the magnetization M or resistivity ρ) is 0.5 for $\text{Mn}_{1.2}\text{Fe}_{2.6}\text{Ga}$ and 0.95 for $\text{Mn}_{1.5}\text{Fe}_{0.9}\text{Ga}$. The sample with the lowest Fe amount shows a H_c of $0.9 \cdot 10^4$ Oe and a squareness ratio of 0.97. In summary, it can be stated that the coercive field and the squareness ratio increases with increasing Mn and decreasing Fe amount. The saturation magnetization of $\text{Mn}_{2-x}\text{Fe}_y\text{Ga}$ is in the range of $M_s \approx 100$ kA/m and $M_s \approx 400$ kA/m depending on the stoichiometry (Fig. 7). Samples with low Fe concentration show a feature in the AGM curves around 0 Oe field, which could not be observed via AHE measurements. This was attributed to a second phase (soft magnetic) inside the Mn-Fe-Ga thin film, which has a different coercive field. At low fields the soft magnetic phase starts to dominate and leads to a sudden increase or decrease of the magnetization. Such behavior was already observed for $\text{Mn}_2\text{Fe}_1\text{Ga}$ samples. [15] Since the AHE measurements do not show such a feature, the anomalous Hall coefficient of the two phases needs to be of a similar value. The Hall resistivity consist of two contributions: $\rho_{yx} = R_0H + R_S4\pi M_S$, where R_0 is the ordinary Hall coefficient and R_S the anomalous Hall coefficient. Since the shape of the magnetization and the AHE hysteresis curves is similar, the AHE prevails the ordinary Hall effect. The same behavior was observed for Mn_{3-x}Ga samples. [16] An overview and a comparison of the measured magnetization with the resistivity ρ_{yx} , conductivity σ_{xy} and the Hall coefficient R_H is given in Fig. 7. All samples show high resistivity (values between 100 and 500 $\mu\Omega$ cm), which can be attributed to the island growth, the high roughness or atomic disorder inside the films. The resistivity increases or decreases proportional to the magnetization and antiproportional to the conductivity, calculated by $\sigma_{xy} = \rho_{yx}/(\rho_{xx}^2 + \rho_{yx}^2)$. Atomic disorder also results in decreased compensation of the magnetic moments of the Mn and Fe atoms, leading to increased magnetization. To increase the applicability of Mn-Fe-Ga as an electrode in MTJ's a TiN seed-layer (30 nm thickness) was used. TiN

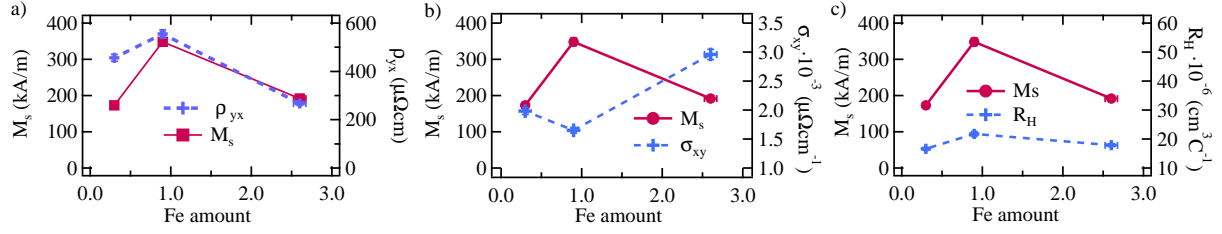


Fig. 7. Comparison of magnetization M with the a) resistivity, b) conductivity and c) Hall constant dependence of Mn-Fe-Ga on the amount of Fe inside of the composition.

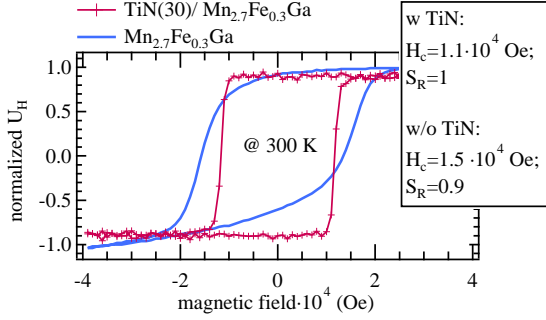


Fig. 8. AHE hysteresis curves of TiN buffered (red) and unbuffered (blue) Mn-Fe-Ga measured at room temperature. Both samples were deposited on MgO substrates. The TiN seed-layer is 30 nm thick.

buffered $Mn_{2.7}Fe_{0.3}Ga$ revealed sharper switching of the magnetization compared to the unbuffered layers (Fig. 8).

IV. CONCLUSION

Structural, magnetic and electrical properties of sputter deposited Mn-Fe-Ga compounds were investigated. The crystallinity of the Mn-Fe-Ga thin films (40 nm thickness) was confirmed using x-ray diffraction. XRR and AFM measurements were utilized to investigate the surface properties, roughness, thickness and density of the deposited Mn-Fe-Ga. Depending on the stoichiometry, as well as the used substrate (STO (001) and MgO (001)) or buffer layer (TiN) the Mn-Fe-Ga crystallizes in the cubic DO_3 ($c = 5.95 \text{ \AA}$) or the tetragonally DO_{22} distorted phase ($c = 7.15 \text{ \AA}$). The main drawback for applications is the island growth, which was confirmed via AFM measurements. Low roughness (≤ 1 nm) and the DO_{22} phase was observed for each used deposition temperature and composition of the Mn-Fe-Ga on STO, whereas on MgO substrates the roughness showed strong dependence on the deposition temperature and the Mn-Fe-Ga composition. Strong PMA was confirmed via AHE and AGM measurements. Low saturation magnetization with values between $M_s \approx 100$ kA/m and $M_s \approx 400$ kA/m and high coercivity fields (up to $H_c \leq 2 \cdot 10^4$ Oe) in the out-of-plane direction were reached by tuning the composition. Temperature dependent AHE measurements in a closed cycle He-cryostat showed a slight increase in coercivity with decreasing temperature (300 K to 2 K). TiN buffered $Mn_{2.7}Fe_{0.3}Ga$ revealed sharper switching of the magnetization compared to the unbuffered layers. The future goal is to integrate the Mn-Fe-Ga into magnetic tunnel junctions and to investigate the applicability of this compound for spin-transfer-torque and magnetic storage devices.

APPENDIX A

The Hall coefficient was calculated via:

$$R_H = \frac{U_H}{B} \cdot \frac{d}{I_x} \cdot \frac{L}{W} \quad (1)$$

with U_H/B the mean value of the measured Hall resistance at maximum positive and negative magnetic field B , respectively. $d = 40$ nm is the film thickness, $I = 100 \mu A$ the used current, $L = 2.5$ mm and $W = 1$ mm are the dimensions of the Hall-structure.

ACKNOWLEDGMENTS

The authors gratefully acknowledge financial support by the Deutsche Forschungsgemeinschaft (DFG, Contract No. RE 1052/32-1).

REFERENCES

- [1] S. A. Wolf, *Science*, vol. 294, no. 5546, p. 1488, 2001.
- [2] G. Reiss and D. Meyners, *Journal of Physics: Condensed Matter*, vol. 19, no. 16, 2007.
- [3] A. Thomas, D. Meyners, D. Ebke, N.-N. Liu, M. D. Sacher, J. Schmalhorst, G. Reiss, H. Ebert, and A. Hütten, *Applied Physics Letters*, vol. 89, no. 1, 2006.
- [4] B. Balke, G. H. Fecher, J. Winterlik, and C. Felser, *Applied Physics Letters*, vol. 90, no. 15, p. 152504, 2007.
- [5] J. Winterlik, B. Balke, G. Fecher, C. Felser, M. Alves, F. Bernardi, and J. Morais, *Physical Review B*, vol. 77, no. 5, p. 12, 2008.
- [6] S. Wurmehl, H. C. Kandpal, G. H. Fecher, and C. Felser, *Journal of Physics: Condensed Matter*, vol. 18, no. 27, p. 6171, 2006.
- [7] M. Glas, C. Sterwerf, J.-M. Schmalhorst, D. Ebke, C. Jenkins, E. Arenholz, and G. Reiss, *Journal of Applied Physics*, vol. 114, no. 18, p. 183910, 2013.
- [8] J. Winterlik, S. Chadov, A. Gupta, V. Alijani, T. Gasi, K. Filsinger, B. Balke, G. H. Fecher, C. A. Jenkins, F. Casper, J. Kübler, G.-D. Liu, L. Gao, S. S. P. Parkin, and C. Felser, *Physical Review B*, vol. 85, no. 47, p. 6283, 2012.
- [9] L. Wollmann, S. Chadov, J. Kübler, and C. Felser, *Physical Review B*, vol. 90, no. 21, p. 214420, 2014.
- [10] C. Felser, V. Alijani, J. Winterlik, S. Chadov, and A. K. Nayak, *IEEE Transactions on Magnetics*, vol. 49, no. 2, p. 682.
- [11] F. Magnus, A. S. Ingason, S. Olafsson, and J. T. Gudmundsson, *Thin Solid Films*, 2011.
- [12] Y. Krockenberger, S.-i. Karimoto, H. Yamamoto, and K. Semba, *Journal of Applied Physics*, vol. 112, no. 8, p. 083920, 2012.
- [13] M. Pritschow, Ph.D. dissertation, Institut für Mikroelektronik Stuttgart, 2007.
- [14] A. Niesen, M. Glas, J. Ludwig, R. Sahoo, D. Ebke, E. Arenholz, J.-M. Schmalhorst, and G. Reiss, *arXiv:1510.06256*, 2015.
- [15] T. Gasi, A. K. Nayak, J. Winterlik, V. Ksenofontov, P. Adler, M. Nicklas, and C. Felser, *Applied Physics Letters*, vol. 102, no. 202402, 2013.
- [16] M. Glas, D. Ebke, I. M. Imort, P. Thomas, and G. Reiss, *Journal of Magnetism and Magnetic Materials* 333, p. 134, 2013.